ICONHIC2022
3rd International Conference on Natural Hazards & Infrastructure
5-7 July 2022, Athens, Greece

An experimental investigation of the seismic behaviour of anchored steel sheet pile walls in saturated sand.

Alessandro Fusco, MSc., Giulia Viggiani, Prof., Gopal S. P. Madabhushi, Prof.
University of Cambridge, Cambridge, UK

Riccardo Conti, Dr.
Università Niccolò Cusano, Roma, Italy

Cécile Prüm, MSc.
ArcelorMittal, Global Research & Development, Esch-sur-Alzette, Luxembourg

ABSTRACT

Several cases are reported of damages caused by earthquake-induced liquefaction to Anchored Steel Sheet Pile (ASSP) walls employed in port facilities. Reliable predictions of the performance of flexible retaining structures under seismic actions require a deeper understanding of their failure mechanisms. This paper presents an experimental investigation of the seismic response of ASSP retaining walls in saturated medium dense sand. Dynamic centrifuge tests on a reduced scale model of an ASSP wall were performed on the Turner beam Centrifuge at the Schofield Centre, Cambridge University. Digital image correlation was used to measure soil displacements in a cross section of the model, providing further insight in the complex soil-structure interaction phenomena occurring. Increasingly stronger seismic signals were applied to the model, to achieve critical conditions gradually. Excess pore pressures generated during seismic shaking play a crucial role in the behaviour of the system, modifying the failure mechanism depending on their extent. In the work, results are presented in terms of bending moments along the wall, anchor forces, excess pore pressures in the backfill, and wall and soil displacements.

Keywords: anchored retaining walls, earthquakes, liquefaction, failure mechanism

INTRODUCTION

Anchored Steel Sheet Pile (SSP) walls are widely used as retaining structures in ports and waterfront facilities due to the ease of installation and limited costs with respect to other types of retaining structures. Because of the large amount of highly seismic coastal areas around the world (*e.g.*, Japan, California, Turkey), the design of anchored SSP walls often requires seismic actions to be included. However, the behaviour of these structures when subjected to seismic shaking is rather complex, as it depends on the interaction between soil and structural elements and on the generation of excess pore pressure, possibly leading to liquefaction. The simplified methods used in engineering practice to design anchored SSP walls often rely on pseudo-static limit equilibrium solutions or subgrade reaction methods. These introduce strong simplifications of the mechanics of the problem to include the development of excess pore pressure and the dynamic thrust of pore fluid on the wall. A more accurate design may be achieved employing dynamic numerical analyses, but these require careful calibration to produce trustworthy results, especially when the excess pore pressure build-up is of interest.

Centrifuge modelling provides an opportunity to study boundary value problems in a controlled environment, giving confidence that the stress-strain relationship of the soil is being evoked at an effective confining stress matching the one at prototype scale. Therefore, the real behaviour of the soil and failure mechanism of the

system are captured. This paper presents the preliminary results of a centrifuge test performed on an anchored SSP wall in uniform medium dense saturated sand. Digital image correlation was used to track the displacement of soil and structure in a cross section of the model. This permitted to obtain novel insight on the failure mechanism of these systems.

EXPERIMENTS LAYOUT

A centrifuge test on a small-scale model of an anchored SSP wall in uniform medium dense saturated sand was performed on the Turner beam centrifuge at the Schofield Centre, University of Cambridge. The model was prepared on the lab floor and then the centrifugal acceleration was gradually increased to 60*g*. Fig. 1 shows the typical layout of an anchored SSP wall and Table 1 summarizes the geometrical dimensions adopted for the model described in this paper.

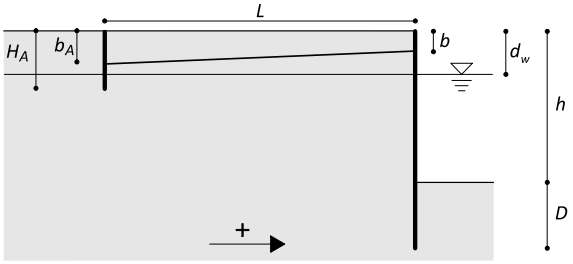

Figure 1. *Typical layout of an anchored SSP wall and sign convention on positive acceleration and displacement.*

Table 1. *Geometry of the centrifuge test. Dimensions at prototype scale, in* [m].

	h	**D**	**b**	**b_A**	**H_A**	**L**	**d_w**
AF07	7	3	0.5	0.5	2	17	2

Centrifuge tests preparation

Modelling a small scale anchored SSP wall

The anchor wall and the main wall were modelled using 4.7 mm thick aluminum plates, matching the bending stiffness of a prototype AZ28 profile. The wall was instrumented with six strain gauges (SG) along its height to measure bending moments, and with four Micro Electrical Mechanical Systems accelerometers (MEMS) to record the horizontal acceleration of the wall. Two tie-backs were created using steel cables passing through holes in the aluminum plates and fixed at their ends using miniature clamps, to guarantee hinged connections. Each tie-back was instrumented with one load cell (LC) to record the anchor force. Transparent plastic sheets were attached to the vertical sides of the two plates to avoid any friction caused by sand particles stuck between the plates and the vertical sides of the container, as this would disturb plane strain conditions.

The soil and pore fluid

The model was prepared by air pluviating Hostun sand (G_S = 2.65, e_{max} = 1.011, e_{min} = 0.555, ϕ_{cr} = 33°) inside the container at a relative density of approximately 50% using an automatic sand pourer (Chian et al, 2010). The model was saturated using a high viscosity aqueous solution of hydroxypropyl methylcellulose (60 cSt) to equate the time of dynamic events and the seepage time (Madabhushi, 2015). Soil accelerations and pore pressures were measured using piezoelectric accelerometers (Acc) and pore pressure transducers (PPTs). Fig. 2 shows the layout of the instrumentation.

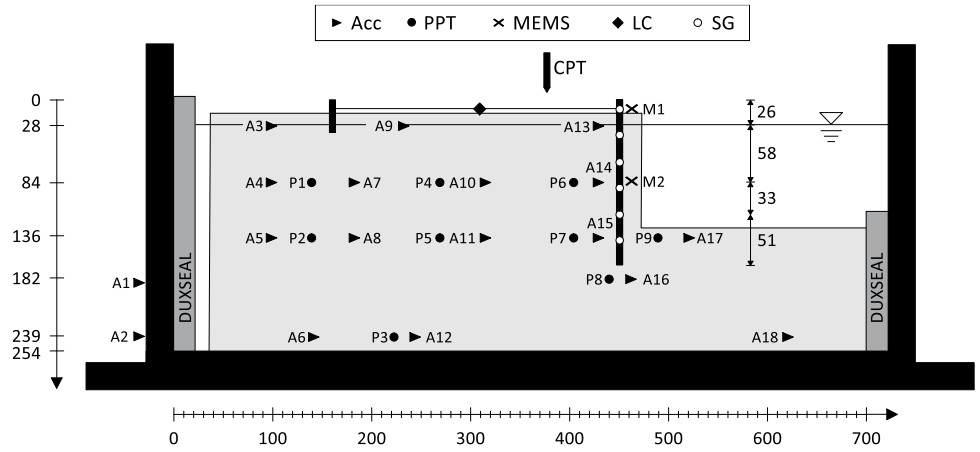

Figure 2. *Instruments layout for centrifuge Test AF07 (dimensions at model scale, in mm).*

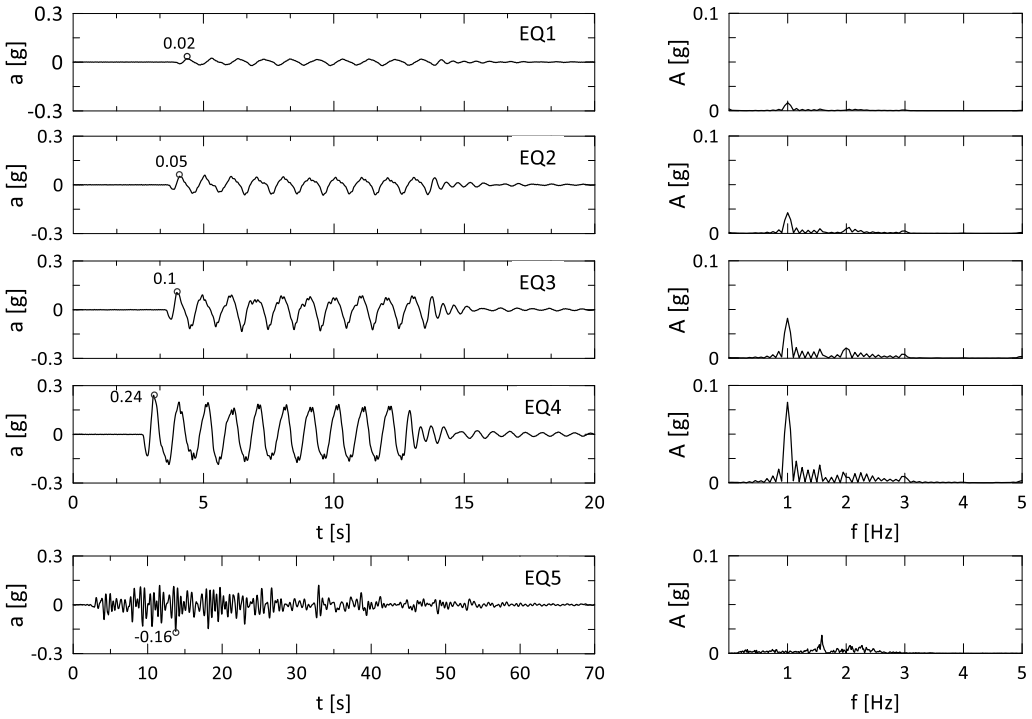

Figure 3. *Acceleration time histories and Fourier amplitude spectra of the earthquakes applied during the centrifuge test (dimensions at prototype scale).*

Container and input motion

The centrifuge test was conducted in a rigid container with internal dimensions of $W \times H \times D = 730 \times 398 \times 250$ mm^3 and a Perspex transparent side, which allowed to perform digital image correlation. A 25 mm thick layer of Duxseal was placed on the vertical lateral boundaries of the container to minimize energy reflection (Steedman & Madabhushi, 1991). Soil and wall displacements were obtained using particle image velocimetry (PIV) analyses conducted using GeoPIV-RG (Stainer et al, 2015). Images of the cross section of the model were captured using a fast digital camera with a frame rate of 975 Hz.

Fig. 3 shows the horizontal acceleration time histories and Fourier amplitude spectra of the seismic signals applied to the model during the centrifuge test. The first four earthquakes consisted of trains of ten nearly sinusoidal cycles with increasing peak acceleration and the same main frequency, equal to 1 Hz. The last input motion applied to the model was the horizontal acceleration time history recorded during the Imperial Valley earthquake (dominant frequency of 1.6 Hz), scaled to 0.16g. The earthquakes were applied to the model using a servo-hydraulic actuator (Madabhushi et al, 2012).

EXPERIMENTAL OBSERVATIONS

In the following, all dimensions are given at prototype scale unless stated otherwise.

Pore pressure and liquefaction

Pore pressure build-up and dissipation

Fig. 4 shows the excess pore pressure time histories recorded along a column of instruments in the far-field (PPTs p1 and p2), in the backfill (PPTs p4 and p5), and in the soil immediately behind the main wall (PPTs p6 and p7) columns during earthquake EQ4. The vertical effective confining stress at the beginning of each earthquake acting on the PPTs, together with the base motion, are also shown.

The excess pore pressure, Δu, measured by PPTs p1, p4 and p6 reaches approximately 40 kPa after the very initial cycles of shaking, and then oscillates around this value. A similar trend is observed for the excess pore pressures measured by PPTs p2 and p5, which, however, increase to about 65 kPa before reaching a plateau. Moreover, the excess pore pressure measured in the soil immediately behind the main wall (PPT p7) stops increasing after reaching approximately 65 kPa. In this case, the generation of excess pore pressure required a larger number of shaking cycles, approximately 6, before achieving a plateau.

In the soil immediately behind the retaining wall, the dissipation of excess pore pressure starts after a few second from the end of the earthquake. Moving further away from the main wall, the excess pore pressure dissipates much slower, starting approximately 10 s and 19 s after the end of the earthquake in the backfill and in the far-field, respectively. The dissipation time in the soil close to the main wall was possibly affected by the presence of the excavation, which provided additional drainage. This may have affected also the generation of excess pore pressure during the earthquake, as it was proved by Adamidis and Madabhushi (2018) that seepage can occur in Hostun sand also during seismic shaking.

Liquefaction

The excess pore pressure ratio, $r_u = \Delta u/\sigma'_{v0}$, resulting from all excess pore pressures shown in Fig.4 is approximately 0.8. This indicates that, during earthquake EQ4, liquefaction was achieved in the soil down to a depth of at least 8.5 m. Fig. 5 shows the acceleration time histories recorded along a column of piezoelectric accelerometers in the backfill, together with the excess pore pressures measured at the nearest location available.

The soil softening resulting from the large generation of excess pore pressures in the backfill, and the consequent drop in the effective confining stress, partially isolated shallower layers of soil from the base motion. This caused significant de-amplification of the acceleration as the shear waves travelled towards the ground surface, as shown in Fig. 5. Incidentally, accelerometers a10 and a11 show high frequency acceleration spikes, which can be attributed to dilation occurring in the sand (Holzer and Youd, 2007).

The maximum excess pore pressure ratio resulting from the reading of PPT p3, at the base of the model, was approximately 0.65, indicating a more limited softening of the soil occurring at depth. In fact, the acceleration recorded in the soil at the base of the model (accelerometer a6) is essentially the same of the applied input motion (accelerometer a2).

Earthquake induced structural displacement and forces.

Structural displacements

Fig. 6 shows the position of the anchor wall and of the main wall at the end of every earthquake applied during Test AF07. At the end of earthquake EQ2, the top of the wall displaced about 0.06 m and its toe about 0.02 m, corresponding to an outward rotation of 0.4%. The rotation of the anchor wall after the same earthquake was larger, or about 2.2%.

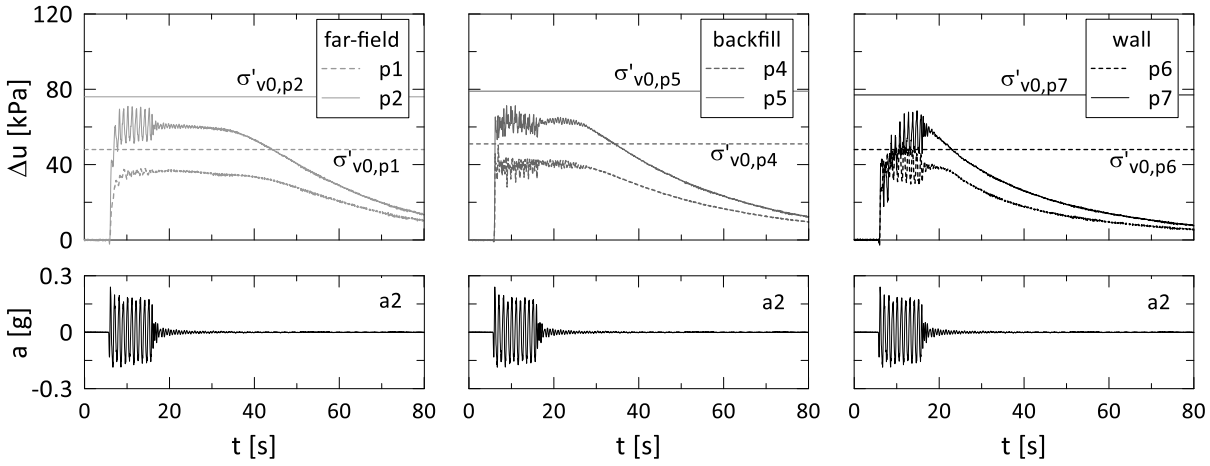

Figure 4. *Excess pore pressure build-up and base acceleration recorded by accelerometer a2 during Test AF07, earthquake EQ4.*

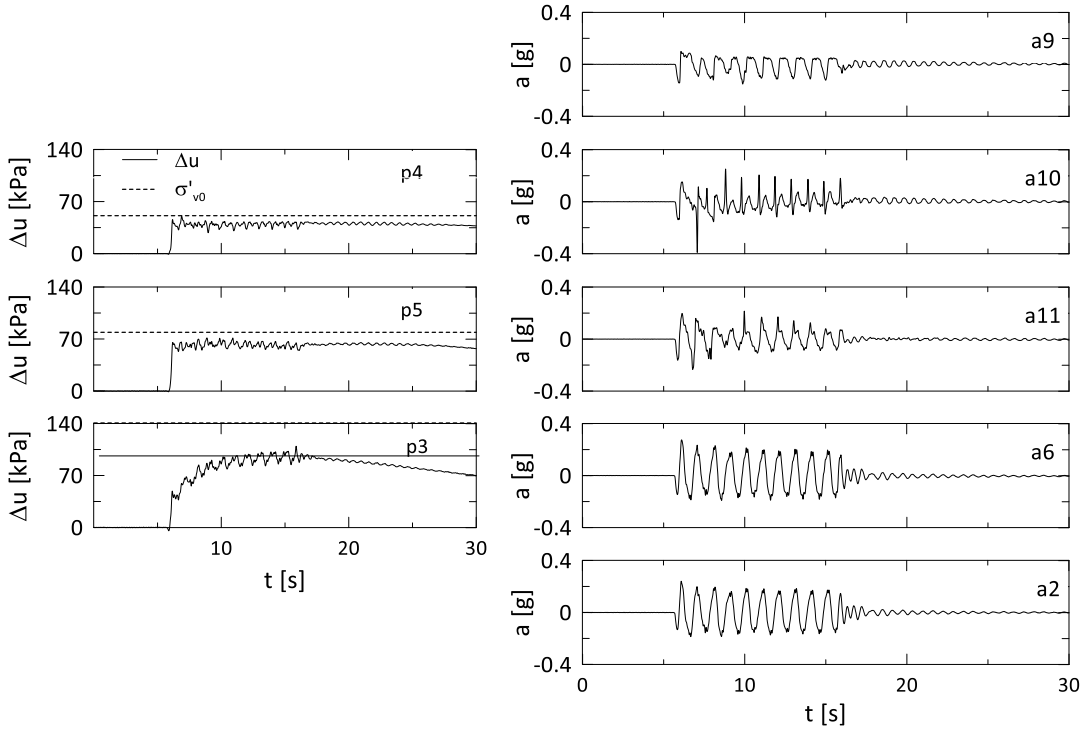

Figure 5. *Excess pore pressure and horizontal acceleration time histories recorded along an array of accelerometers and PPTs in the backfill (Test AF07, earthquake EQ4).*

Earthquakes EQ3 and EQ4 were the most destructive events, which caused the generation of large excess pore pressure in the soil. The top of the wall displaced by about 0.8 m and 1.65 m during earthquakes EQ3 and EQ4, respectively, and also the toe of the wall accumulated significant horizontal displacement, approximately 0.4 m and 0.8 m, that is 50% and 48% of the displacement of the top of the main wall, for earthquakes EQ3 and EQ4 respectively. These figures indicate a different behaviour from what observed by Fusco et al. (2019) on anchored SSP walls in dry sand, which experienced very limited displacements at the toe of the main wall, regardless of the magnitude of displacement of the top. In the saturated tests, the significant displacement of the toe of the wall can be attributed to softening of the soil around the embedded part of the wall caused by the accumulation of excess pore pressures.

The rotation of the main wall at the end of earthquakes EQ3 and EQ4 was 3.9% and 13.1%, respectively, and the rotation of the anchor wall during the same earthquakes was extremely severe, approximately 24% after earthquake EQ3 and increasing to 70% after EQ4. At the end of earthquake EQ5 the top of the main wall displaced horizontally by about 0.5 m. However, in this case the toe of the wall stayed nearly in place. The

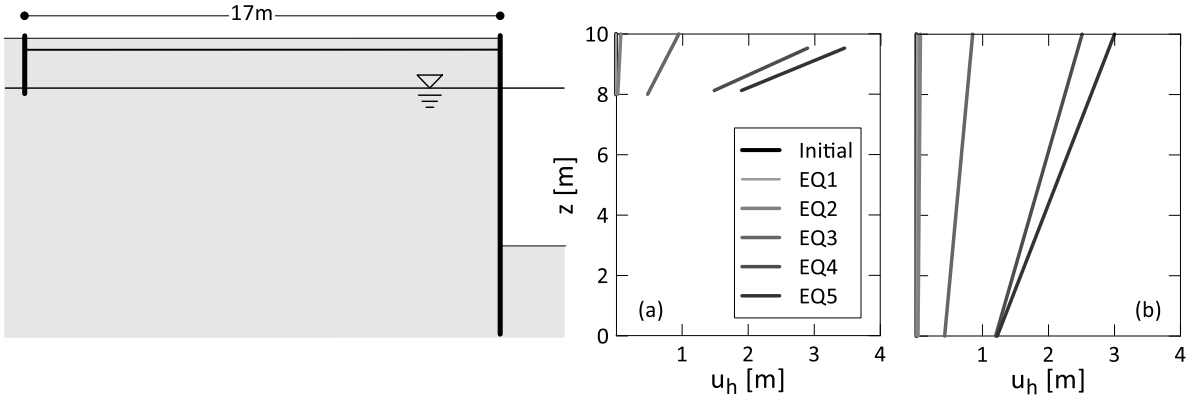

Figure 6. *(a) Position of anchor and (b) retaining wall at the end of all earthquakes applied during Test AF07 (left: layout of the test).*

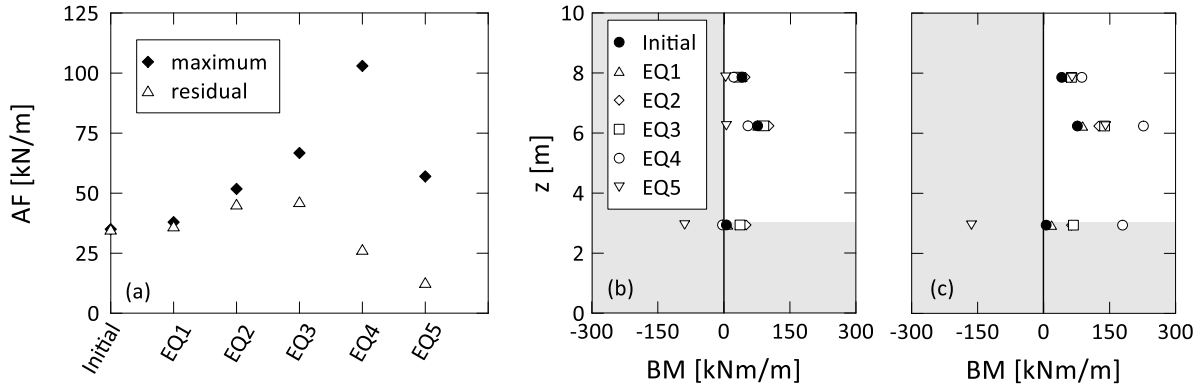

Figure 7. *(a) Maximum and residual anchor force, AF, in the tiebacks, (b) residual and (c) envelope of the maximum bending moment, BM, on the wall for all earthquakes applied during Test AF07.*

final outward rotation of the wall after earthquake EQ5 was therefore 17%, about 30% larger than the rotation of the wall identified after earthquake EQ4, whereas the final rotation of the anchor wall was approximately 70%, about 10% more the rotation of the anchor wall measured at the end of the previous earthquake, EQ4.

Anchor forces and bending moments

Fig. 7(a) shows the anchor force, AF, measured on the tie-backs immediately after swing-up (static), together with the maximum and residual anchor force recorded respectively during and at the end of every applied earthquake. Fig. 7(b) shows the initial and residual bending moment measured along the main wall and Fig. 7(c) shows the envelope of maxima of the recorded bending moment along the wall. Due to instrument malfunctioning during the test, the readings of three strain gauges were not available. Therefore, only measurements from the remaining strain gauges are presented. The residual forces and bending moments refer to the measurements recorded after complete dissipation of excess pore pressures.

During the first four earthquakes applied, the maximum anchor force always increased with the amplitude of the applied input motion, and the same was observed for maximum bending moments. The maximum anchor force measured during earthquake EQ4 is about 100 kN/m, approximately three times larger than the static anchor force. Similarly, the maximum bending moment recorded during EQ4, approximately 226kNm/m, is about three times larger than the static bending moment.

Residual anchor forces and bending moments are recorded in the tie-backs during the first three earthquakes applied, consistently with what observed by other authors (Zeng & Steedman, 1993; Madabhushi & Zeng, 2007). At the end of earthquake EQ3, the anchor force is approximately 30% higher than the static anchor force, whereas the residual bending moment recorded by SG4 in the main wall is 18% larger than the static value. During the last two seismic events the trend changes. The residual anchor force recorded at the end of earthquake EQ4 is 44% smaller than at the end of the previous earthquake, and it reduces even further after earthquake EQ5, reaching a final value of 12kN/m. This is approximately one third of the static anchor force.

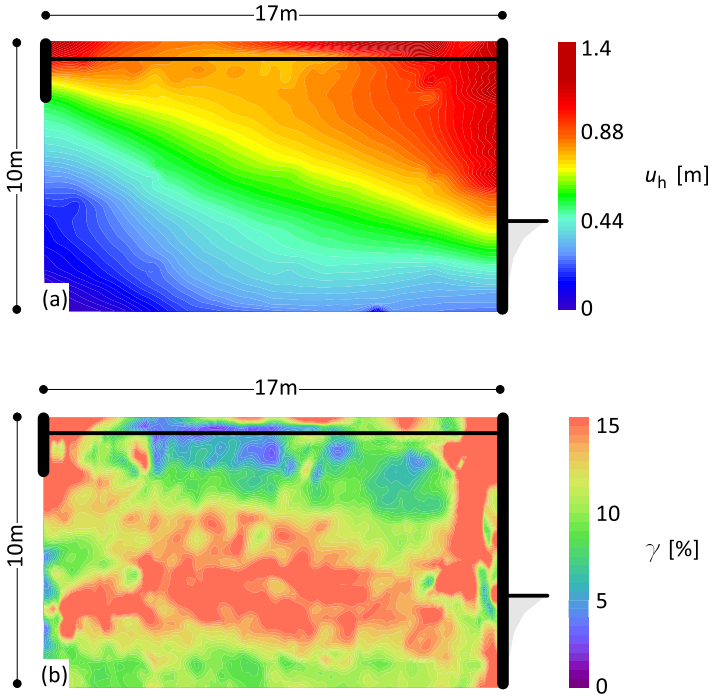

Figure 7. *(a) Horizontal displacement contours and (b) shear strain of a cross section of the model, during earthquake EQ4, Test AF07.*

Similarly, the residual bending moment recorded by SG4 reduces to about 70% and 1% of the static value, after earthquakes EQ4 and EQ5, respectively.

During earthquake EQ5, the maximum bending moment was no longer recorded at 4 m depth, as for all previous seismic events, but it occurred at dredge level, with a value of -160kNm/m. Consistently with what observed for the peak values, at the end of the same earthquake, the maximum residual bending moment was measured at dredge level, rather than at mid-height of the wall as at the end of previous earthquakes.

The significant reduction of residual anchor forces recorded after earthquake EQ5, and the large increase of negative bending moment at dredge level during the same earthquake, reveals a different behaviour of the main wall from that observed during previous earthquakes. During the same earthquake, also the displacement mode of the main wall (Fig. 6(b)) is different from the general trend observed for previous earthquakes, in that the horizontal displacement of the toe of the wall is very limited. These results suggest that, during earthquake EQ5, the displacements of the toe of the wall were restrained. Possible causes of that were sand particles trapped in the gap between the model wall and the sides of the container.

Failure mechanisms

Fig. 8(a) and show the contours of horizontal displacement of the soil in the backfill obtained from particle image velocimetry analyses for earthquake EQ4, and Fig. 8(b) shows the shear strain contours for the same earthquake.

Consistently with the horizontal displacements of the main wall in Fig. 6, horizontal displacements of the soil larger than 1.3 m occur in the soil immediately behind the main wall and in front of the anchor wall. The wedge of soil delimited by the anchor wall and the main wall, and above a surface extending from approximately the toe of the anchor wall to dredge level, on the main wall, experienced an approximately uniform horizontal displacement field. The shear strain occurring in the failing soil wedge is limited, whereas significant shear strain occurs below the failure surface. This confirm the nearly uniform displacement field experienced by the failing soil wedge, which is a typical characteristics of global failure mechanisms, as described by (Caputo et al, 2019).

CONCLUSIONS

A centrifuge test was carried out on a small scale model of an anchored steel sheet pile wall in medium dense saturated sand, to investigate the response of these type of retaining structures under seismic actions. Both sinusoidal motions and real earthquakes were used as base excitations. During strong earthquakes, significant excess pore pressures generated in the backfill. This led to liquefaction of the retained soil, resulting in a strong de-amplification of seismic waves, as they travelled towards the ground surface, and severe horizontal displacements of the system. Approaching the main wall, excess pore pressures dissipated faster, indicating two dimensional seepage effects, which may have also affected the generation of excess pore pressures in the retained soil.

Particle image velocimetry analyses allowed the measurement of the displacement field and shear strain of a cross section of the model. The horizontal displacement field of the soil and shear strains developed in the backfill allowed to identify the failure mechanism of the system, as corresponding to global failure.

REFERENCES

Adamidis, O. , Madabhushi, S. P. G. (2018). Experimental investigation of drainage during earthquake-induced liquefaction. Géotechnique, 68(8), 655-665.

Caputo, G , Conti, R , Viggiani, G.M.B , Prüm, C. (2019). Theoretical framework for the seismic design of anchored steel sheet pile walls. In Proceedings of the 7th International Conference on Earthquake Geotechnical Engineering, ICEGE, 2019.

Chian, S. C., Stringer, M. E., & Madabhushi, S. P. G. (2010, June). Use of automatic sand pourers for loose sand models. In Proceedings of the 7th International Confefernce on Physical Modelling of Geotechnics (pp. 117-121). Rotterdam, Netherlands: CRC Press.

Conti, R. , Madabhushi, G. S. P. , Viggiani, G. M. B. (2012). On the behaviour of flexible retaining walls under seismic actions. Géotechnique, 62(12), 1081-1094.

Fusco, A. , Viggiani, G. M. B. , Madabhushi, S. P. G. , Caputo, G. , Conti, R. , Prüm, C. (2019, January). Physical modelling of anchored steel sheet pile walls under seismic actions. In Earthquake Geotechnical Engineering for Protection and Development of Environment and Constructions-Proceedings of the 7th International Conference on Earthquake Geotechnical Engineering, 2019 (pp. 2502-2509).

Holzer, T. L. and Youd, T. L. (2007). Liquefaction, ground oscillation, and soil deformation at the wildlife array, california. Bulletin of the Seismological society of America, 97(3):961–976.

Madabhushi, G. (2014). Centrifuge modelling for civil engineers. CRC Press.

Madabhushi, G. S. , Haigh, S. K. , Houghton, N. E. , Gould, E. (2012). Development of a servo-hydraulic earthquake actuator for the Cambridge Turner beam centrifuge. International Journal of Physical Modelling in Geotechnics, 12(2), 77-88.

Madabhushi, S. P. G. , Zeng, X. (2007). Simulating seismic response of cantilever retaining walls. Journal of Geotechnical and Geoenvironmental Engineering 133(5), 539–549.

Stanier, S. A. , Blaber, J. , Take, W. A. , White, D. J. (2015). Improved image-based deformation measurement for geotechnical applications. Canadian Geotechnical Journal, 53(5), 727-739.

Steedman, R. S. , Madabhushi, S. P. G. (1991). Wave transmission at a multi-media interface. In Proceedings of the 5th International Conference on Soil Dynamics and Earthquake Engineering. Elsevier.

Zeng, X. (1990). Modelling the behaviour of quay walls in earthquakes. PhD thesis, University of Cambridge, UK.

Zeng, X. , Steedman, R. S. (1993). On the behaviour of quay walls in earthquakes. Geotechnique, 43(3), 417-431.